Metal-insulator-metal antennas in the far-infrared range based on highly doped InAsSb

F. Omeis, Rafik Smaali, F. Gonzalez-Posada, Laurent Cerutti, Thierry Taliercio, E. Centeno

Metal-insulator-metal antennas in the far-infrared range based on highly doped InAsSb

F. Omeis, R. Smaali, F. Gonzalez-Posada, L. Cerutti, T. Taliercio, and E. Centeno

Citation: Appl. Phys. Lett. **111**, 121108 (2017); doi: 10.1063/1.4995515
View online: http://dx.doi.org/10.1063/1.4995515
View Table of Contents: http://aip.scitation.org/toc/apl/111/12
Published by the American Institute of Physics

Metal-insulator-metal antennas in the far-infrared range based on highly doped InAsSb

F. Omeis,[1,2] R. Smaali,[1,2] F. Gonzalez-Posada,[3,4] L. Cerutti,[3,4] T. Taliercio,[3,4] and E. Centeno[1,2]
[1]*Université Clermont Auvergne, Institut Pascal, BP 10448, F-63000 Clermont-Ferrand, France*
[2]*CNRS, UMR 6602, Institut Pascal, F-63177 Aubière, France*
[3]*Université Montpellier, IES, UMR 5214, F-34000 Montpellier, France*
[4]*CNRS, IES, UMR 5214, F-34000 Montpellier, France*

(Received 12 July 2017; accepted 11 September 2017; published online 22 September 2017)

Plasmonic behavior in the far-infrared (IR) and terahertz (THz) ranges can facilitate a lot of applications in communication, imaging or sensing, security, and biomedical domains. However, simple scaling laws cannot be applied to design noble metal-based plasmonic systems operating at far-IR or THz frequencies. To overcome this issue, we numerically and experimentally explore the plasmonic properties in the spectral range between 25 and 40 μm (12 and 7.5 THz) of metal-insulator-metal (MIM) antennas made of InAsSb a highly Si-doped semiconductor. We demonstrate that these MIM antennas sustain a gap plasmon mode that is responsible for high light absorption. By tracking this peculiar plasmonic signature for various antennas' widths, we prove that Si-doped InAsSb microstructures realized on large areas by laser lithography and the wet etching process are a low cost, reproducible, and readily CMOS compatible approach. *Published by AIP Publishing.*
[http://dx.doi.org/10.1063/1.4995515]

In the last few decades, plasmonic systems have attracted increasing interest owing to their ability to enhance and confine free-space electromagnetic waves into subwavelength regions. Among the various plasmonic geometries studied such as the bow-tie, the v-antenna, and the stacked optical antenna,[1–4] Metal-Insulator-Metal (MIM) resonators are particularly attractive. They have been demonstrated to boost the Purcell factor and the light extraction or to behave as perfect and tunable absorbers.[5,6] The majority of plasmonic resonators including MIM antennas are utilized in the visible to near-infrared (IR) (400–2000 nm) where several application domains such as biosensing or photovoltaics benefit on the plasmonic effects.[7–10] Extending the use of plasmonics in the far-(IR) and terahertz (THz) ranges becomes crucial for the next communication, imaging, sensing, security, and biomedical applications.[11–15] However, the development of plasmonic systems operating in the far-IR and THz is still facing challenges concerning their fabrication. Indeed, plasmonic effects arise when photons and electrons strongly interplay, which requires an operating frequency close enough to the plasma frequency of the metals. Since the plasma frequency of noble metals is typically in the ultraviolet spectrum of light, plasmonic interaction is weak at the THz frequencies, and these materials are considered as perfect electric conductors (PECs). In addition, the strong dispersion of the optical properties (refractive index and absorption coefficient) of Drude metals prevents applying simple scaling laws for transposing any plasmonic architectures from the visible to the THz ranges.[16] Moreover, intraband free carrier losses degrade the optical efficiency of these plasmonic systems in far-IR. At last, silver or gold is not compatible with the CMOS technology, which prevents their straightforward integration. In sum, all these constrains explain why it is challenging to shift plasmonic resonances of MIM antennas beyond the near-IR range[11,16–19] except in some extreme geometrical conditions.[20]

To overcome the material barriers that prevent us from simply scaling the MIM resonators in the far-IR, appropriate materials presenting a metallic behavior from far-IR to THz ranges are thus needed. A study of inter-metallic compounds to find the ideal plasmonic material had been made to reduce the losses, but the degree of controlling losses is still a constraint.[21] Alkali metals are also a good candidate for low-loss plasmonic structures, but they are very reactive to air and water which make them dangerous substances and therefore prohibit their fabrication.[22] Therefore, using highly doped semiconductors (HDSCs) is an elegant approach to realize metal-like materials in the desired range of frequency since the plasma frequency, which depends on the electronic density, can be adjusted by controlling the doping level.[23,24] In addition to their easy tunability, HDSCs are compatible with CMOS technology, making them good candidates for future commercial applications. Recent works have highlighted different kinds of HDSC plasmonic behaviours in the infrared ranges based on doped silicon,[25] GaAs,[26] germanium,[27] and InAs.[28–30]

In this letter, we report an experimental demonstration of plasmonic MIM antennas made of HDSCs that operate in the far-IR. As shown in Fig. 1(a), the MIM resonators are made of a GaSb dielectric spacer of thickness g and dielectric permittivity $\varepsilon_d = 13.4$,[31] sandwiched between a back mirror and a periodic set of antennas made of silicon doped InAsSb with pitch d, thickness h, and width w. The relative permittivity of InAsSb is described by the Drude model

$$\varepsilon_{InAsSb} = \varepsilon_\infty \left(1 - \frac{\omega_p^2}{\omega(\omega + i\gamma)}\right), \tag{1}$$

where $\varepsilon_\infty = 10.4$, $\gamma = 10^{13}\,\mathrm{rad\,s^{-1}}$, and the plasma frequency $\omega_p = 351 \times 10^{12}\,\mathrm{rad\,s^{-1}}$ are experimentally determined by measuring the Brewster mode.[32] In order to minimize the electromagnetic coupling between adjacent MIM antennas,

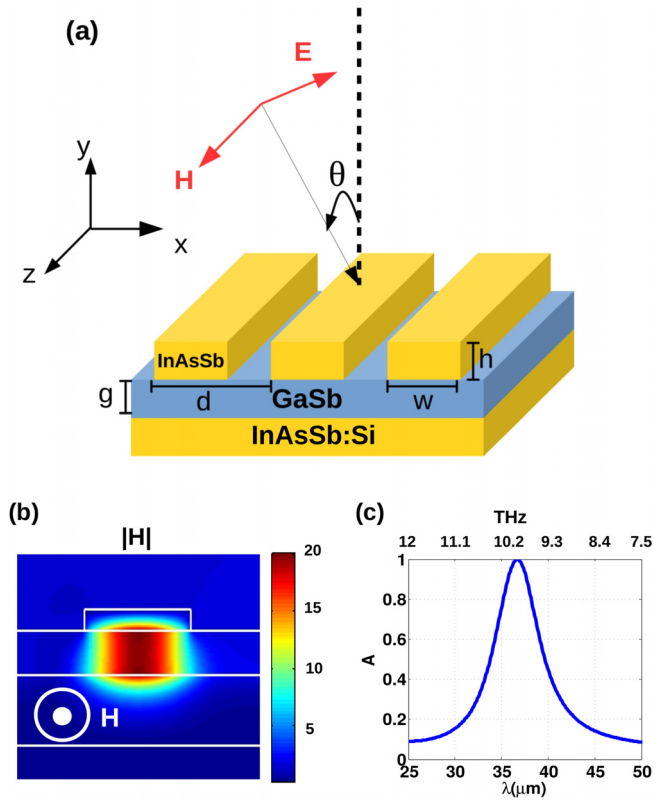

FIG. 1. (a) Schematic of MIM resonators consisting of InAsSb strips, a GaSb spacer, and a InAsSb:Si back reflector. (b) Map of the modulus of the magnetic field calculated at the resonant wavelength of the gap plasmon mode. (c) Absorption spectra for MIM resonators whose parameters are $d = 10\,\mu$m, $w = 3\,\mu$m, $g = 0.63\,\mu$m, and $h = 0.3\,\mu$m.

we use a period $d = 10\,\mu$m, which is 3 times larger than the antennas' width.

In this framework, the incident electromagnetic wave with a magnetic field polarized along the antenna arrays couples into a plasmonic mode, named gap-plasmon, guided in the dielectric spacer [Fig. 1(b)]. When the thickness of the spacer is reduced to only hundredths of the wavelength, the gap-plasmon is slowed down; meanwhile, its effective index increases according to the approximated analytical formula

$$n_{eff} = \sqrt{\varepsilon_d}\sqrt{1 + \frac{2\delta_p}{g}}, \tag{2}$$

where δ_p is the skin depth of the metal.[34,35] It is possible to reach perfect absorption because the Fabry-Perot resonance in the MIM antennas behaves as a cavity for the gap plasmon.[33] The fundamental resonant wavelength λ_r is directly linked to the width w of the antenna and the effective index of the gap plasmon.[36] This model allows one to derive a simple expression for λ_r

$$\lambda_r = 2n_{eff}w + \lambda_\phi, \tag{3}$$

where λ_ϕ is a correction phase term. The resonance can be shifted by a demand by playing with the width w of the antennas and the thickness g of the spacer. For example, we observe an absorption peak at $\lambda_r = 37\,\mu$m for a transverse magnetic wave at normal incidence for antennas of width $w = 3\,\mu$m and height $h = 0.3\,\mu$m on a spacer of thickness $g = 0.63\,\mu$m [Fig. 1(c)]. Here, the absorption coefficient A is calculated by applying the following equation: $A = 1 - R - T$, where R and T are the reflection and transmission coefficients calculated using a home-made code based on the rigorous coupled-wave analysis method (RCWA).[37] This resonant wavelength can be predicted easily by calculating the effective index ($n_{eff} = 4.9$) of the mode and replacing it in Eq. (3) with a correction phase term. Remark that the dynamical modification of the carrier concentration into the HDSC using, for example, the photogeneration process paves an interesting avenue for realizing tunable MIM antennas that could be used for spectrometry in the far-IR and THz.[38,39]

We fabricated an all semiconductor MIM antenna array to demonstrate experimentally the efficient absorption through the gap plasmon coupling with THz waves. The gap plasmon structure has been grown by solid source molecular beam epitaxy (RIBER, compact 21 growth chamber). The growth procedure is an oxide desorption of the Te-doped (100)-GaSb substrate, followed by a deposited mirror of 993 nm of Si doped $InAs_{0.9}Sb_{0.1}$ with a carrier concentration of $5 \times 10^{19}\,cm^{-3}$, which allows us to reach a metallic behaviour for frequency lower than 54 THz. The spacer of 630 nm thickness is a non-intentional doped (nid) GaSb. Finally, a thinner layer of 298 nm of highly doped n-$InAs_{0.9}Sb_{0.1}$ with the same doping level is grown in which the antennas are fabricated by laser lithography and wet chemical etching. We used AZMIR-701 photoresist spun at 4000 rpm for 30 s and heated at 90 °C for 1 min. The laser lithography equipment uses an ultraviolet laser at $\lambda = 365$ nm. The power and the writing speed were optimized to obtain samples of $2 \times 2\,mm^2$ surfaces with different periods and antenna widths for each. The angular-dependent reflectance measurements of the plain InAsSb layers lattice-matched onto the GaSb substrate shows a dip in the reflection spectrum at $0.182\,\mu m^{-1}$ (5.5 μm), which corresponds to the Brewster mode.[32]

The reflectance spectra have been obtained using a Bruker V70 Fourier Transform Infrared (FTIR) spectrometer equipped with a Potassium bromide (KBr) beam splitter, a Far Infrared Radiation (FIR) source, and a Si-bolometer cooled to 4.2 K. The experimental setup allows us to cover the spectral range from 15 to 55 μm. The $2 \times 2\,mm^2$ surface was studied for each sample. The incident beam makes an angle of 60° with the normal of the surface. A holographic wire grid polarizer has been used to polarize the incident light. The antennas' widths are measured by scanning electron microscopy (SEM). Figures 2(a) and 2(b) show the

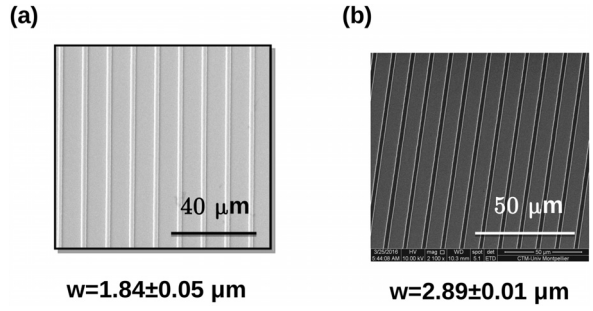

FIG. 2. SEM images of the InAsSb:Si grating of widths (a) $w = 1.84 \pm 0.05\,\mu$m and (b) $w = 2.89 \pm 0.01\,\mu$m.

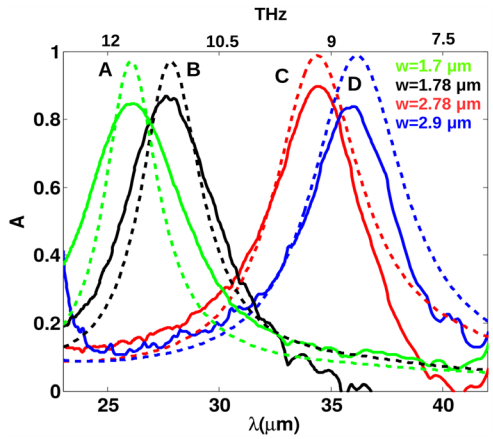

FIG. 3. Experimental data (solid lines) compared to the simulated results (dashed) for different widths of the antennas for four samples of widths $w = 1.7$, 1.78, 2.78, and 2.9 μm.

antennas of widths $w = 1.84 \pm 0.05\ \mu$m and $w = 2.89 \pm 0.01\ \mu$m. We have extracted absorption spectra from reflectance measurements by assuming a zero transmittance because of the back mirror.

Figure 3 shows the absorption spectra for samples with similar geometrical parameters: $d = 10\ \mu$m, $g = 0.63\ \mu$m, and $h = 0.298\ \mu$m. The experimental spectra (solid curves) are in a good agreement with the simulated ones. We observe a slight decrease in the absorption lines attributed to the geometrical imperfections which are weak for a large surface ($2 \times 2\,\text{mm}^2$). However, more importantly, the spectral position of the experimental absorption line is red shifted when the width of the MIM resonators is increased according to the Fabry-Perot model for the gap plasmon. As seen in Fig. 4, the experimental fundamental resonant wavelength λ_r is a linear function of the width w of the MIM antenna as described in Eq. (3). Here, the error bars indicate the statistical error between the overall width of the antennas fabricated in each sample. According to Fig. 4, the slope of the experimental graph allows us to deduce the gap plasmon's effective index ($n_{eff} \simeq 4.7$), which in turn predicts the approximate value of the theoretical thickness of the GaSb spacer for the samples.

Note that tuning the resonances of the gap plasmon mode by just changing the width of the antennas is an easy

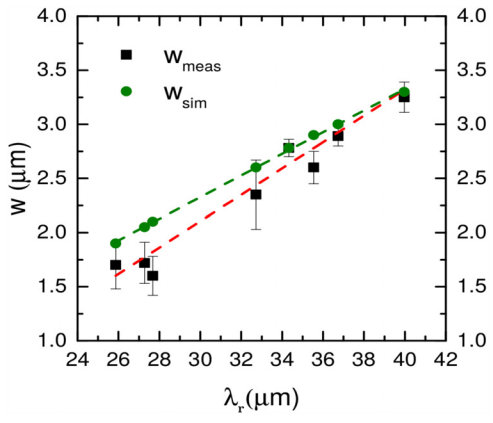

FIG. 4. The linear behaviour of the resonant wavelength λ_r with the width of the resonator w according to the experimental and simulated data.

TABLE I. Comparison of the experimental and simulated Q factors for samples A, B, C, and D.

	Sample A	Sample B	Sample C	Sample D
Q_{exp}	4.65	5.4	6.8	6.9
Q_{sim}	7.2	7.3	6.5	7.05

and reproducible step in the laser lithographic procedure. These results allow us to reach the subwavelength scalability and tunability of HDSC MIM resonators in the THz range, which cannot be achieved using noble metals.

In order to compare the performance of the HDSC-based MIM antennas operating in the far-IR to those made of noble metals that operate in the visible range, we analyze the quality factor $Q = \lambda_r/\Delta\lambda$, where $\Delta\lambda$ is the full width at half maximum of the absorption line. The Q-factor is a qualitative characteristic of MIM resonators, which is related to the absorption and scattering losses and determines their efficiency. First, both experimental and the simulated Q factors for samples A, B, C, and D are close to an average error value less than 15% [Table I]. These values are comparable with the state of art for MIM antennas made of noble metals.[40–42] Our results demonstrate that the electromagnetic properties of our HDSC-based MIM resonators are similar to those of their metallic counterpart and that gap plasmon resonances can be efficiently transposed in the far-IR.

In conclusion, we have demonstrated the potential of InAsSb:Si and GaSb materials to realize MIM antenna arrays which support gap-plasmon resonances up to THz frequencies (~7 THz). This approach allows us to reach near perfect absorption in the far-IR spectral range by easily adjusting the antenna geometry. The spectral positions of the gap plasmon resonances and their corresponding quality factors extracted from the absorption measurements in the far-IR are equivalent to those accomplished with noble metals in the visible range. These results show that HDSC-based MIM antennas are a flexible CMOS compatible technology and might lead to significant improvements for various far-IR and THz applications such as sensing, imagery, and security.

[1]J. N. Farahani, H.-J. Eisler, D. W. Pohl, M. Pavius, P. Fluckiger, P. Gasser, and B. Hecht, Nanotechnology **18**, 125506 (2007).
[2]L. Lin and Y. Zheng, Sci. Rep. **5**, 14788 (2015).
[3]M. F. G. Klein, H. Jein, P.-J. Jakobs, S. Linden, N. Meinzer, M. Wegener, V. Saile, and M. Kohl, Microelectron. Eng. **86**, 1078 (2009).
[4]A. Saeed, S. Panaro, R. P. Zaccaria, W. Raja, C. Liberale, M. Dipalo, G. C. Messina, H. Wang, F. De Angelis, and A. Toma, Sci. Rep **5**, 11237 (2015).
[5]G. M. Akselrod, C. Argyropoulos, T. B. Hoang, C. Ciraci, C. Fang, J. Huang, D. R. Smith, and M. H. Mikkelsen, Nature Photon. **8**, 835 (2014).
[6]J. Hao, L. Zhou, and M. Qiu, Phys. Rev. B **83**, 165107 (2011).
[7]Y. Chu, D. Wang, W. Zhu, and K.-B. Crozier, Opt. Exp. **19**(16), 14919 (2011).
[8]A. Cattoni, P. Ghenuche, A.-M. Haghiri-Gosnet, D. Decanini, J. Chen, J.-L. Pelouard, and S. Collin, Nano Lett. **11**, 3557 (2011).
[9]N. Vandamme, H.-L. Chen, A. Gaucher, B. Behaghel, A. Lemaitre, A. Cattoni, C. Dupuis, N. Bardou, J.-F. Guillemoles, and S. Collin, IEEE J. Photovoltaic **5**, 565 (2015).
[10]F. Bigourdan, F. Marquier, J.-P. Hugonin, and J.-J. Greffet, Opt. Exp. **22**(3), 2337 (2014).
[11]H.-H. Chen, H.-H. Hsiao, H.-C. Chang, W.-L. Huang, and S.-C. Lee, Appl. Phys. Lett **104**, 083114 (2014).
[12]J.-F. Federici, B. Schulkin, F. Huang, D. Gary, R. Barat, F. Oliveira, and D. Zimdars, Semicond. Sci. Technol. **20**, S266–S280 (2005).

[13]G. Liang, X. Hu, X. Yu, Y. Shen, L.-H. Li, A. Giles Davies, E.-H. Linfield, H.-K. Liang, Y. Zhang, S.-F. Yu, and Q.-J. Wang, ACS Photonic **2**, 1559 (2015).
[14]E. Pickwell and V.-P. Wallace, J. Phys. D: Appl. Phys. **39**, R301 (2006).
[15]S. Koenig, D. Lopez-Diaz, J. Antes, F. Boes, R. Henneberger, A. Leuther, A. Tessmann, R. Schmogrow, D. Hillerkuss, R. Palmer, T. Zwick, C. Koos, W. Freude, O. Ambacher, J. Leuthold, and I. Kallfass, Nat. Photonics **7**, 977 (2013).
[16]G. Isić and R. Gajić, J. Appl. Phys. **116**, 233103 (2014).
[17]D. Palaferri, Y. Todorov, Y. N. Chen, J. Madeo, A. Vasanelli, L. H. Li, A. G. Davies, E. H. Linfield, and C. Sirtori, Appl. Phys. Lett. **106**, 161102 (2015).
[18]C. Koechlin, P. Bouchon, F. Pardo, J.-L. Pelouard, and R. Haidar, Opt. Express **21**, 7025 (2013).
[19]H. Hang, Y. Li, and Y. Yong-Hong, Chin. Phys. Lett. **31**, 018101 (2014).
[20]R. Smaali, F. Omeis, A. Moreau, T. Taliercio, and E. Centeno, Sci. Rep. **6**, 32589 (2016).
[21]M. G. Blaber, M. D. Arnold, and M. J. Ford, J. Phys. Condens. Matter **21**, 144211 (2009).
[22]M. G. Blaber, M. D. Arnold, N. Harris, M. J. Ford, and M. B. Cortie, Physica B **394**, 184 (2007).
[23]V. N'Tsame Guilengui, L. Cerutti, J. B. Rodriguez, E. Tournie, and T. Taliercio, Appl. Phys. Lett. **101**, 161113 (2012).
[24]A. J. Hoffman, L. Alekseyev, S. S. Howard, K. J. Franz, D. Wasserman, V. A. Podolskiy, E. E. Narimanov, D. L. Sivco, and C. Gmachl, Nat. Mater. **6**, 946–950 (2007).
[25]J. C. Ginn, R. L. Jarecki, Jr., E. A. Shaner, and P. S. Davids, J. Appl. Phys. **110**, 043110 (2011).
[26]M. Fehrenbacher, S. Winnerl, H. Schneider, J. Doring, S. C. Kehr, L. M. Eng, Y. Huo, O. G. Schmidt, K. Yao, Y. Liu, and M. Helm, Nano Lett. **15**, 1057 (2015).
[27]J. Frigerio, A. Ballabio, G. Isella, E. Sakat, G. Pellegrini, P. Biagioni, M. Bollani, E. Napolitani, C. Manganelli, M. Virgilio, A. Grupp, M. P. Fischer, D. Brida, K. Gallacher, D. J. Paul, L. Baldassarre, P. Calvani, V. Giliberti, A. Nucara, and M. Ortolani, Phys. Rev. B **94**, 085202 (2016).
[28]S. Law, D. C. Adams, A. M. Taylor, and D. Wasserman, Opt. Express **20**, 12155 (2012).
[29]F. Barho, F. Gonzalez-Posada, M.-J. Milla-Rodrigo, M. Bomers, L. Cerutti, and T. Taliercio, Opt. Express **24**(14), 16175 (2016).
[30]M.-J. Milla, F. Barho, F. Gonzalez-Posada, L. Cerutti, M. Bomers, J.-B. Rodriguez, E. Tournié, and T. Taliercio, Nanotechnology **27**, 425201 (2016).
[31]S. Roux, P. Barritault, O. Lartigue, L. Cerutti, E. Tournie, B. Grard, and A. Grisard, Appl. Phys. Lett. **107**, 171901 (2015).
[32]T. Taliercio, V. Ntsame Guilengui, L. Cerutti, E. Tournie, and J.-J. Greffet, Opt. Express **22**(20), 24294 (2014).
[33]S.-I. Bozhevolnyi and T. Sodergaard, Opt. Express **15**(17), 10869 (2007).
[34]S. Collin, F. Pardo, and J.-L. Pelouard, Opt. Express **15**, 4310 (2007).
[35]F. Pardo, P. Bouchon, R. Haidar, and J.-L. Pelouard, Phys. Rev. Lett. **107**, 093902 (2011).
[36]J. Yang, C. Sauvan, A. Jouanin, S. Collin, J.-L. Pelouard, and P. Lalanne, Opt. Express **20**(15), 16880 (2012).
[37]T. Weiss, G. Granet, N. A. Gippius, and S. G. Tikhodeev, Opt. Express **17**, 8051 (2009).
[38]Y. Yang, N. Kamaraju, S. Campione, S. Liu, J. L. Reno, M. B. Sinclair, R. P. Prasankumar, and I. Brener, ACS Photonics **4**, 15 (2017).
[39]R. Smaali, T. Taliercio, and E. Centeno, Opt. Lett. **41**, 3900 (2016).
[40]T. Xu, Y. K. Wu, X. Luo, and L. J. Guo, Nat. Commun. **1**, 59 (2010).
[41]N. Liu, M. Mesch, T. Weiss, M. Hentschel, and H. Giessen, Nano Lett. **10**, 2342 (2010).
[42]A. Moreau, C. Ciraci, J. J. Mock, R. T. Hill, Q. Wang, B. J. Wiley, A. Chilkoti, and D. R. Smith, Nature **492**(7427), 86 (2012).